# Nonlinear elasto-plastic performance prediction of materials stabilized with bitumen emulsion in rural road pavements

Ignacio Pérez[a*], Luis Medina[a], Miguel Angel del Val[b]
[a] Universidade da Coruña, E. T. S. I. Caminos, Campus de Elviña, 15071 A Coruña, Spain.
*Corresponding author. Tel: (+34) 981.167.000-Ext. 1451. Fax: (+34) 981.167.170.
[b] Technical University of Madrid - UPM, Department of Civil Engineering-Transport, Ciudad Universitaria, 28040 Madrid, Spain.
E-mail addresses: iperez@udc.es (Ignacio Pérez), lmedina@udc.es (Luis Medina), miguel.delval@upm.es (Miguel Angel del Val).

**Abstract**

This article presents numerical modelling of rural road pavement sections recycled in situ with two materials stabilized with bitumen emulsion. The two materials stabilized with bitumen emulsion are base course materials comprising 25% reclaimed asphalt pavement and 75% natural aggregates with and without 1% cement. A 3D-finite difference model was used to determine the response of these pavement sections when subjected to two types of loads with four types of soil subgrades of varying resistances. A nonlinear elasto-plastic Mohr-Coulomb model was used in the two materials stabilized with bitumen emulsion, and a nonlinear model was adopted in the four soil subgrades. Both the resilient and permanent behaviours of these materials were modelled. An analysis was conducted on rutting and fatigue resistances of the base course materials. The base course material containing 1% cement is more resistant and is apt for use in lightly trafficked rural roads. Both base course materials stabilized with bitumen emulsion will first fail from rutting before fatigue.

**Keywords:** pavement analysis; 3D finite difference model; FLAC3D; nonlinear, pavement recycling; rehabilitation; bitumen emulsion.

## 1. Introduction

One of the primary goals of highway administrations is to maintain the road network in an optimal state of repair and operation. A large part of these networks is composed of lightly trafficked rural roads that use flexible pavements constructed with thin wearing courses comprising asphalt materials and base courses fabricated with unbound granular materials

resting upon soil subgrades of relatively low resistance. One of the most effective actions for the maintenance of these pavements was found to be in situ treatment of recycled pavement with bitumen emulsion. In keeping with this convention, the process known as Full Depth Reclamation (**FDR**) is a rehabilitation technique in which the full thickness of an asphalt wearing course and a predetermined portion of an underlying unbound granular base course are uniformly milled, pulverized and blended to provide a new base course material stabilized with bitumen emulsion (**BSM**) [1].

In recent years, research on **BSM** has focussed mainly on characterisation, formulation and implementation. Significant progress has been made in these fields. However, relatively little ground has been gained in the study of the mechanical behaviour of **BSM** for improving the structural design of the rehabilitation solutions. Most of the methods used to analyse structural designs do not consider the specific mechanical characteristics of **BSM**. A number of different researchers have reported that these materials play a structural role that varies between the application range of unbound granular materials and the asphalt mixes [2-4]. In this sense, **BSM** exhibits a nonlinear behaviour similar to that of unbound granular materials, which depends on the pavement stress states, with the most critical mechanical property being shear stress resistance [3-5]. In other words, the failure of these materials is mainly due to significant permanent deformation (rutting) that has an irreversible and negative effect on the structural and functional state of the pavement [2].

The objective of this article is to determine the pavement responses at critical positions in two rural roads pavement sections with **BSM** base courses. For this purpose, a 3D-finite difference model will be used considering the **BSM**-specific mechanical characteristics. The permanent deformation (rutting) produced in the **BSM** will be attained. In addition, fatigue resistance will be analysed.

## 2. Pavement Analysis Model

### *2.1. 3D Finite Difference Model*

Two three-layer system sections are modelled (Fig. 1). The first section was studied earlier in South Africa [3]. It consists of a Hot Mix Asphalt **(HMA)** wearing course 40 mm thick overlying a **BSM** base course 200 mm thick placed directly over the subgrade. South Africa typically rehabilitates roads with 40 mm **HMA** wearing courses and 200 mm **BSM** base courses. This type of rehabilitation specifically belongs to category **C**: rural roads that are lightly trafficked or strategic roads. These roads have an 80% design reliability and 0.3 to 1 million equivalent standard axle loads (0.3 to 1 **MESA**) [6]. The second section is similar but with an **HMA** wearing course 80 mm thick. This second section is not used in the South Africa roads and is analysed for comparison with the first section.

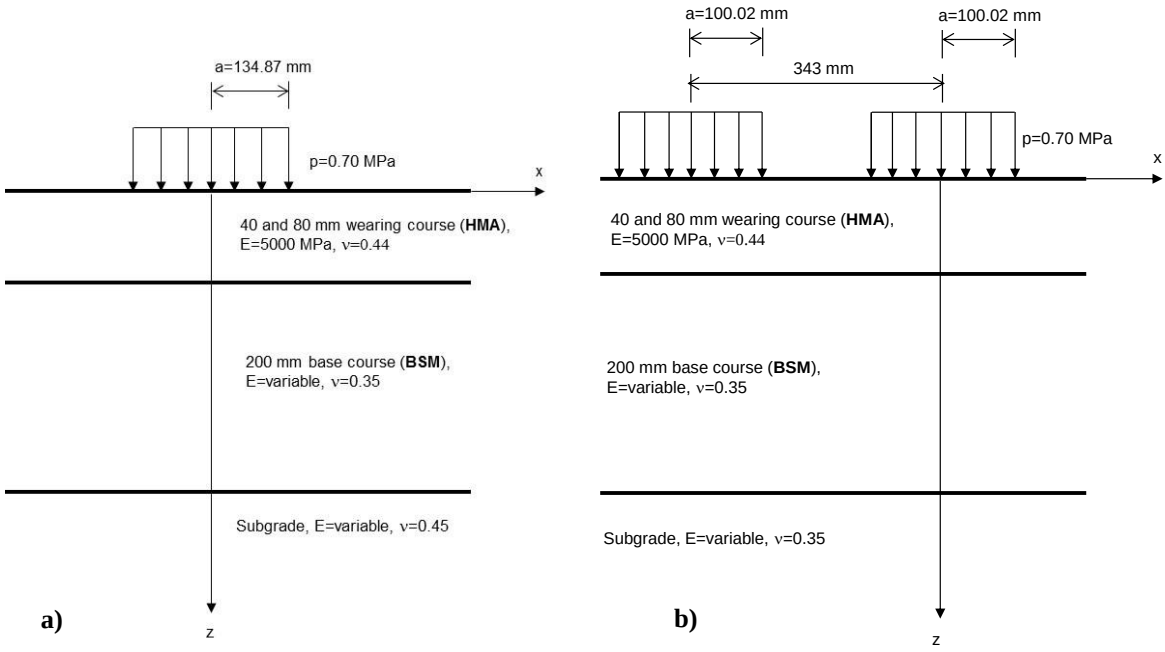


**Fig. 1**. Pavement structure used for modelling: a) Single tire (**ST**), b) Dual tyres (**DT**).

On the other hand, the permissible axle load in South Africa of a single axle with dual wheels is 88 kN, whereas the permissible axle load of a single axle with single wheels used as steering axle is 77 kN, and that of a single axle with single wheels that is not a steering axle is 80 kN [7]. Therefore, two load configurations are used: an 80 kN single axle with two single

tyres (**ST**) (Fig. 1a) and a 88 kN single axle with two dual tyres (**DT**) (Fig. 1b). A homogeneous circular load **p**=0.70 MPa with a radius **a**=134.87 mm is applied to the single tyre. For dual tyres, **p** is also 0.70 MPa but with **a**=100.02 mm, and the distance between radial centres is equal to 343.00 mm.

The numerical modelling of the stress state produced in the pavement, created by the application of a static load on its surface, was carried out with the commercial code FLAC3D-3.10 (Fast Lagrangian Analysis of Continua in 3 Dimensions) [8]. This is a three-dimensional code that uses a specific scheme of finite differences that allows the elastic-plastic behaviour of the materials used in pavement layers to be simulated. The materials are represented by polyhedric elements forming a three-dimensional grid that fits the shape of the modelled object. Each element behaves according to an established law of stress-strain (linear or nonlinear) in response to the loads applied and the boundary conditions. Fig. 2 shows the finite difference grid and the coordinate system used for dual tyres. The model comprises 2500 elements and 2900 nodes.

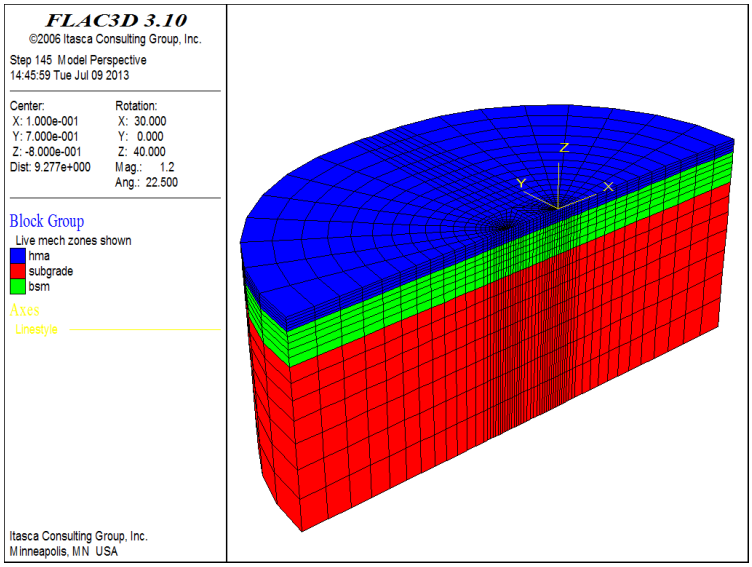


**Fig. 2**. 3D-finite difference grid (40 mm **HMA** wearing course, dual tyres).

Given the conditions of symmetry entailed in the problem (in terms of geometry and loads), only one-fourth of the real problem is studied. The following boundary conditions were applied (Fig. 2):

- Movements prevented in direction 'x' on plane x = 0 (symmetry plane).
- Movements prevented in direction ‘y’ on plane y = 0 (symmetry plane).
- Movements prevented in directions 'x' and 'y' on the lateral (circular) edge of the grid. The lateral (circular) edge of the grid was located far from the load (1.4 m away from the tyre centre) so that it would have a minimal effect on the results.
- All movements prevented on the lower plane $z$ = -1.24 m.

Continuity conditions are satisfied at the layer interfaces. The process reproduced with the numerical model consists of two phases: The first provides the in situ state of stresses existing in the pavement before applying the load. Once the state of mechanical equilibrium has been reached for the specific weights and boundary conditions applied, all movements of the model start out at zero. The load is applied in the second phase.

*2.2. Material Characterization*

*2.2.1. HMA wearing course*

In this research, emphasis should be given to nonlinear elastic-plastic Mohr-Coulomb modelling of the **BSM** base course. In the **HMA** wearing course, a linear elastic behaviour is considered. This layer is characterised by the values of the following parameters: specific weight $\gamma$=24 kN/m$^3$, coefficient of earth pressure at rest $K_0$=0.6, elastic modulus $E$=5000 MPa and Poisson’s coefficient $\nu$=0.44 [3].

*2.2.2. BSM base course*

It is assumed that **FDR**-type treatments are carried out on a pavement that originally consisted of a thin bituminous wearing course and a thick unbound granular base course. Hence, the resulting **BSM** comprises only 25% Reclaimed Asphalt Pavement (**RAP**). Moreover, two different cases are considered: a) 25% **RAP**+75% natural aggregates (**R0**) and b) 25% **RAP**+75% natural aggregates+1% cement (**R1**). These two **BSM** base courses are characterised by the values of the following parameters: $\gamma$=22 kN/m$^3$; $K_0$=0.6 and $\nu$=0.35 [3].

A nonlinear elastic behaviour is assumed [9]. In keeping with this, the well-known $M_r$-$\Theta$ model, initially developed for unbound granular materials, is used to obtain the resilient modulus ($M_r$) of these materials [3]:

$$M_r = k_1 \theta^{k_2} \quad (1)$$

where $\Theta=\sigma_1 +2\sigma_3$, and $\sigma_1$ and $\sigma_3$ are the major and minor principal stresses, respectively. The main drawback of this model is that negative values of $\Theta$ yield incongruent values of $M_r$. Ebels [3] obtained the experimental coefficients $k_1$ and $k_2$ of **R0** and **R1** materials by means of dynamic triaxial tests (Table 1). In Table 1, it may be observed that in material **R0,** the value of parameter $k_1$ is equal to 130 MPa, whereas in material **R1** (stiffer) this parameter is equal to 150 MPa. Parameter $k_2$ is very similar in the two materials.

**Table 1**. **BSM** base course nonlinear model coefficients and shear parameters [3].

| BSM | $M_r$-$\Theta$ Model (25ºC, 2 Hz) | | Mohr-Coulomb (25ºC) | |
|---|---|---|---|---|
| | $k_1$ | $k_2$ | $c$ (MPa) | $\phi$ (º) |
| R0 | 130 | 0.30 | 0.152 | 38.4 |
| R1 | 150 | 0.33 | 0.387 | 29.7 |

Moreover, Table 1 provides the cohesion ($c$) and angle of friction ($\phi$), which allow for the modelling of the elastic-plastic behaviour. According to Jenkins et al. [2], $c$ and $\phi$ determine the shear stress resistance and therefore the permanent deformation resistance. Compared to material **R0**, in material **R1** with 1% cement, $c$ increases and $\phi$ decreases.

*2.2.3. Subgrade*

A fine-grained soil is studied with $\gamma$=20 kN/m$^3$; $K_0$=0.6 y $\nu$=0.45. In this case, a nonlinear elastic model is used in which $M_r$ decreases as $\sigma_d$ increases [10-12]:

$$\begin{aligned} M_r &= k_1 + k_3(k_2 - \sigma_d) \text{ when } \sigma_d \le k_2 \\ M_r &= k_1 - k_4(\sigma_d - k_2) \text{ when } \sigma_d \ge k_2 \end{aligned} \quad (2)$$

where $\sigma_d= \sigma_1-\sigma_3$=deviator stress. Thompson and Elliot [12] obtained the experimental coefficients $k_1$, $k_2$, $k_3$ and $k_4$ of four types of subgrade soils by means of dynamic triaxial tests. In Table 2, the values of these coefficients are listed in the four types of subgrade soils with

various degrees of resistance: **S** (Strong); **M** (Medium); **W** (Weak); **VW** (Very Weak). According to Thompson and Elliot [12] the value of $M_r$ at the point where $k_1$ is equal to $\sigma_d$ (at the curve breakpoint) is a good indicator of the resilient behaviour of the subgrade material. In this sense, the strong subgrade (**S**) exhibits a characteristic $M_r$ of 85.1 MPa, whereas the weakest subgrade (**VW**) has an $M_r$ of only 6.9 MPa.

**Table 2**. Coefficients of subgrade model [12].

| Subgrade soils | $k_1$ (kPa) | $k_2$ (kPa) | $k_3$ | $k_4$ |
|---|---|---|---|---|
| S (Strong) | 85100 | | | |
| M (Medium) | 53000 | 42.8 | 1110 | 178 |
| W (Weak) | 20800 | | | |
| VW (Very Weak) | 6900 | | | |

*2.3. Behaviour models*

The rutting resistance of the **BSM** base course is studied by using a double exponential model that predicts the three phases of the cumulative permanent strain ($\varepsilon_p$) versus the number of load cycles ($N$) [3]:

$$\varepsilon_p = A\left(\frac{N}{1000}\right)^B + C\left(\exp^{D\frac{N}{1000}} - 1\right) \tag{3}$$

$$A = a_1(SR)^{a_2};\ B = b_1(SR)^{b_2};\ C = c_1(SR)^{c_2};\ D = d_1(SR)^{d_2}$$

Ebels [3] obtained the experimental coefficients $a_1$, $a_2$, $b_1$, $b_2$, $c_1$, $c_2$, $d_1$, and $d_2$ of materials **R0** and **R1** by means of dynamic triaxial tests. In Table 3, the values of these eight parameters for materials **R0** and **R1** are listed:

Table 3. **BSM** base course permanent deformation model coefficients (25ºC, 2 Hz) [3].

| BSM | $a_1$ | $a_2$ | $b_1$ | $b_2$ | $c_1$ | $c_2$ | $d_1$ | $d_2$ |
|---|---|---|---|---|---|---|---|---|
| R0 | 0.92 | 1.45 | 0.66 | 1.47 | $1.9 \times 10^{-7}$ | -12.14 | $7.9 \times 10^{0}$ | 8.72 |
| R1 | 2.53 | 2.39 | 2.31 | 2.47 | $4.9 \times 10^{2}$ | 18.09 | $3.3 \times 10^{1}$ | 7.81 |

In equation 3, $SR$ is the so-called Stress Ratio, which is expressed as the ratio between the acting deviator stress ($\sigma_d$) and the deviator stress at failure ($\sigma_{d,f}$) for the Mohr-Coulomb criterion [2,13,14):

$$SR = \frac{\sigma_d}{\sigma_{d,f}} = \frac{\sigma_1 - \sigma_3}{\sigma_3\left[\tan^2\left(45^o + \frac{\phi}{2}\right) - 1\right] + 2c\tan\left(45^o + \frac{\phi}{2}\right)} \tag{4}$$

where $\sigma_1$ and $\sigma_3$ are the major and minor principal stresses in static triaxial tests, respectively.

Jenkins et al [2] reported that *SR* is a critical parameter that defines the mechanical response of **BSM** materials to the permanent deformation (**PD**). As the value of *SR* increases, the $\varepsilon_p$ value goes up as well. According to Jenkins et al [2], when the *SR* value is greater than 0.40, high **PD** (rutting) is produced. It is very important to locate the critical position of *SR* in the layer. To accomplish this, $\sigma_1$ and $\sigma_3$ are determined using the finite difference code at different locations in the **BSM** base course, which allows the calculation of *SR* by means of equation 4. The critical position was considered to be the point yielding the maximum *SR* ($SR_{max}$). This value is used in equation 3 to estimate $\varepsilon_p$.

Moreover, to check the **BSM** fatigue resistance, the following expression is used [15]:

$$N_f = a \ \mu\varepsilon_r^{-n} \tag{5}$$

where $N_f$ is the number of load cycles applied until fatigue failure occurs, and $\mu\varepsilon_r$ is the tensile strain in micrometres that occurs in the **BSM** base course lower fibre.

Twagira et al [15] obtained the experimental coefficients *a* and *n* of materials **R0** and **R1** by means of fatigue tests. Table 4 shows these experimental coefficients for materials **R0** and **R1**.

**Table 4**. **BSM** base course fatigue law coefficients (5ºC, 2 Hz) [15].

| BSM | *a* | *n* |
|---|---|---|
| R0 | $5.01 \times 10^{13}$ | 3.48 |
| R1 | $1.99 \times 10^{20}$ | 6.10 |

## 3. Results and Discussion

### *3.1. Structural Capacity and Pavement Responses*

Two scenarios corresponding to the two pavement sections discussed in section 2.1 are analysed. The first scenario (pavement **P1**) has an **HMA** wearing course 40 mm thick (Fig. 1a), and the second scenario (pavement **P2**) has an **HMA** wearing course 80 mm thick (Fig. 1b). The critical responses of the materials in the pavement structure are studied in terms of

the different qualities of the two **BSM** base courses constructed over subgrades of four fine soils with a resistance range that goes from rigid to very weak. Three variables of the pavement response were monitored at the following critical points (Table 5):

- Tensile strain ($\varepsilon_r$) in the **HMA** wearing course and in the **BSM** base course lower fibres**.**
- Deflection ($d$) on the **HMA** wearing course surface and in the subgrade (**SUBG**) upper fibres.
- Vertical strain ($\varepsilon_v$) in the subgrade (**SUBG**) upper fibre.

**Table 5**. Pavement responses.

| | | | **P1** | | | | | | **P2** | | | | | |
|---|---|---|---|---|---|---|---|---|---|---|---|---|---|---|
| | | | **HMA** | | **BSM** | | **SUBG** | | **HMA** | | **BSM** | | **SUBG** | |
| **Load** | **BSM** | **Soil** | $\varepsilon_r$ (με) | $d$ (mm) | $\varepsilon_r$ (με) | $SR_{max}$ | $\varepsilon_v$ (με) | $d$ (mm) | $\varepsilon_r$ (με) | $d$ (mm) | $\varepsilon_r$ (με) | $SR_{max}$ | $\varepsilon_v$(με) | $d$ (mm) |
| ST | R0 | S | -148 | 0.362 | -309 | 0.975 | 683 | 0.252 | -172 | 0.260 | -189 | 0.628 | 456 | 0.184 |
| | | M | -147 | 0.405 | -340 | 0.975 | 755 | 0.289 | -174 | 0.283 | -203 | 0.742 | 498 | 0.208 |
| | | W | -149 | 0.483 | -380 | 0.983 | 930 | 0.356 | -176 | 0.322 | -226 | 0.891 | 574 | 0.246 |
| | | VW | -152 | 0.549 | -398 | 0.992 | 1379 | 0.409 | -178 | 0.352 | -252 | 0.936 | 674 | 0.274 |
| | R1 | S | -82 | 0.297 | -236 | 0.349 | 583 | 0.225 | -126 | 0.222 | -167 | 0.284 | 402 | 0.166 |
| | | M | -81 | 0.333 | -255 | 0.379 | 655 | 0.261 | -127 | 0.243 | -178 | 0.287 | 437 | 0.187 |
| | | W | -78 | 0.396 | -283 | 0.429 | 816 | 0.323 | -128 | 0.277 | -193 | 0.292 | 594 | 0.221 |
| | | VW | -77 | 0.446 | -302 | 0.466 | 1109 | 0.372 | -129 | 0.303 | -202 | 0.295 | 660 | 0.247 |
| DT | R0 | S | -142 | 0.305 | -138 | 0.782 | 517 | 0.218 | -117 | 0.228 | -98 | 0.441 | 361 | 0.166 |
| | | M | -141 | 0.345 | -150 | 0.901 | 593 | 0.257 | -118 | 0.252 | -108 | 0.452 | 399 | 0.189 |
| | | W | -140 | 0.419 | -176 | 0.937 | 755 | 0.327 | -120 | 0.291 | -122 | 0.540 | 463 | 0.228 |
| | | VW | -139 | 0.480 | -187 | 0.953 | 963 | 0.382 | -121 | 0.320 | -131 | 0.609 | 506 | 0.255 |
| | R1 | S | -93 | 0.259 | -120 | 0.316 | 451 | 0.198 | -93 | 0.199 | -89 | 0.234 | 324 | 0.152 |
| | | M | -92 | 0.295 | -133 | 0.320 | 516 | 0.233 | -93 | 0.220 | -97 | 0.237 | 355 | 0.172 |
| | | W | -90 | 0.358 | -153 | 0.326 | 653 | 0.295 | -94 | 0.255 | -108 | 0.240 | 406 | 0.207 |
| | | VW | -88 | 0.408 | -166 | 0.331 | 834 | 0.343 | -95 | 0.281 | -115 | 0.243 | 445 | 0.232 |

The maximum stress ratio ($SR_{max}$) of the **BSM** base course was also obtained. The following is an explanation of the effect exerted on the above points by the following characteristics:

- **HMA** thickness.
- Load configuration.
- Mechanical properties of both **BSM** base course and subgrade.

*3.1.1. Effect of HMA wearing course thickness*

As expected, the increase of the **HMA** wearing course thickness generally produces

fewer pavement responses. For example, in Fig. 3a and 3b, it can be observed that with both single and dual tyres, the surface deflections on the **HMA** wearing course and in the subgrade upper fibre are consistently fewer in pavement **P2**. This also occurs with the vertical strains in the subgrade upper fibre (Table 5, Fig. 3e). Moreover, Fig. 3c shows that in the **BSM** base course, the tensile strains in the lower fibre that occur in pavement **P2** are always smaller than those produced in **P1**. In addition, Table 5 shows that the $SR_{max}$ values in the **BSM** base course are always lower in pavement **P2**.

However, as seen in Fig. 3d, this does not happen in the **HMA** wearing course, given that in pavement **P2** with a single tyre, the tensile strains in the bottom of the **HMA** wearing course are greater for both **R0** and **R1** materials. The latter occurrence is also observed with dual tyres and **R1** material. To investigate this behaviour, tensile strains of **HMA** thicknesses between 20 mm and 140 mm were calculated. Fig. 4a represents the tensile strain in the **HMA** wearing course bottom versus thickness, with **R0** and **R1** materials, single and dual tyres and strong subgrade. Fig. 4b represents the tensile strain in the **HMA** wearing course bottom versus thickness, with **R0** and **R1** materials, dual tyres and the four subgrade soils. Both figures show an **HMA** critical thickness at which a maximum tensile strain is produced. Below this critical thickness, the tensile strain decreases with decreasing thickness, whereas above the critical thickness, the tensile strain decreases with increasing thickness. This performance was observed before in flexible pavements constructed with **HMA** wearing courses resting upon unbound granular materials [12,16,17]. The explanation of this performance is that above the critical thickness, the wearing course provides an "*elastic structural layer*" action, whereas a thinner layer exhibits "*membrane type*" behaviour [12].

*3.1.2. Effect of load configuration*

The impact on the pavement is generally lower with dual tyres (Table 5). In keeping with this, the deflections produced with dual tyres (**DT**) on the **HMA** surface (Fig. 3a) and in

the subgrade upper fibre (Fig. 3b) are consistently lower than those that occur with single tyres (**ST**). The same is true with the vertical strains in the subgrade upper fibre (Table 5, Fig. 3e). The tensile strains in the **BSM** (Fig. 3c) and **HMA** layers (Fig. 3d) follow this same pattern of behaviour. Moreover, the $SR_{max}$ values in the **BSM** base courses are lower with dual tyres (Table 5).

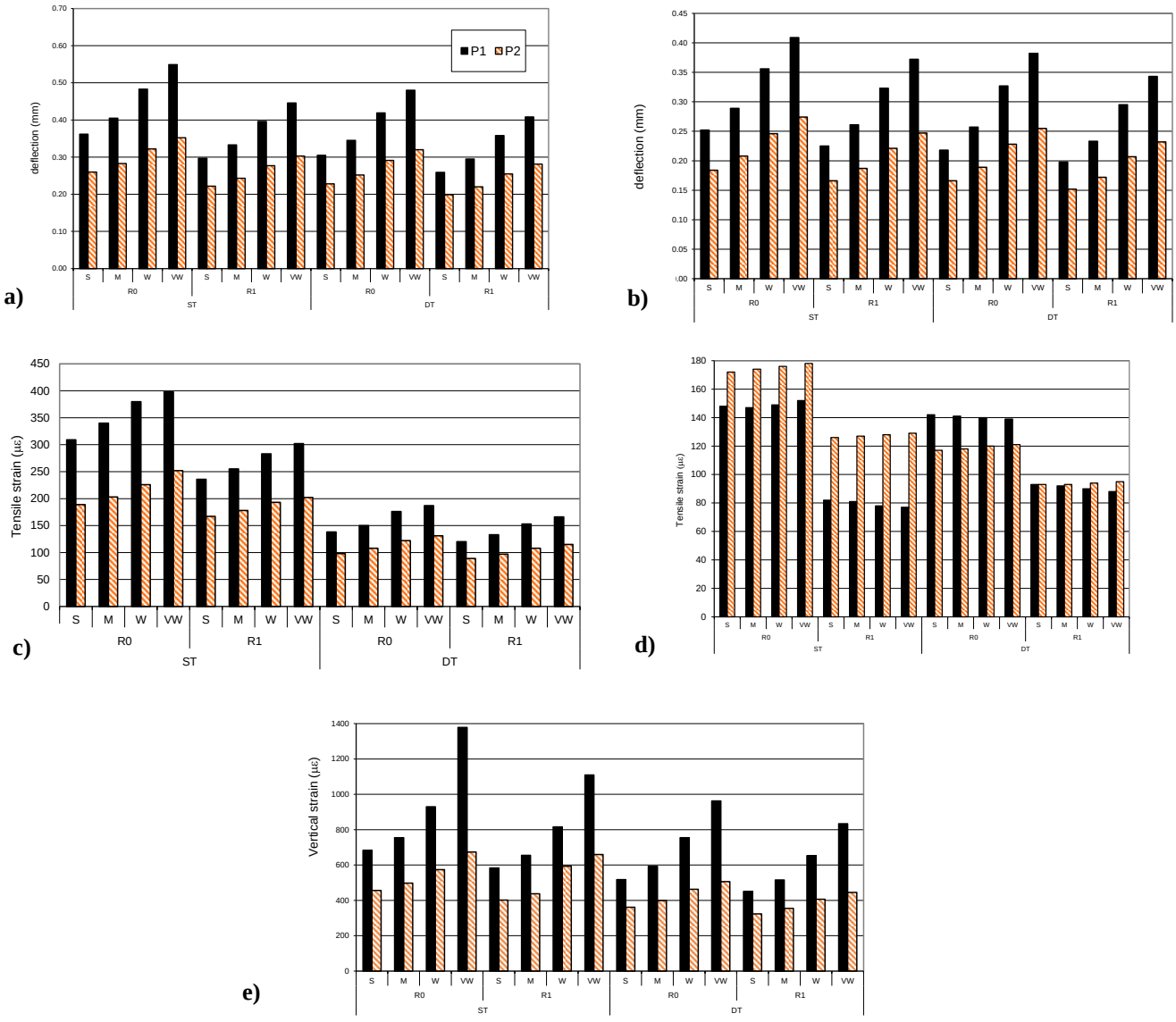


**Fig. 3**. Pavement responses: a) deflections on the **HMA** wearing course surface; b) deflections in the subgrade upper fibre; c) **BSM** base course tensile strain (lower fibre); d) **HMA** wearing course tensile strain (lower fibre); e) vertical strains in the subgrade upper fibre.

As an exception to this behaviour, with **R1** material, the tensile strains in the **P1-HMA** wearing course are higher with **DT** than with **ST** (Fig. 3d). In Fig. 4a, it can be observed that in **R1** material below 50 mm, the replacement of **ST** by **DT** increases the tensile strain. The

same is observed in **R0** material below 40 mm. This behaviour results because with thin wearing courses, the **ST** load generates greater stresses in the **BSM**. Therefore, in accordance with equation 1, the resilient modulus increases, making the **BSM** base course stiffer and producing a decrease of the **HMA** wearing course tensile strains.

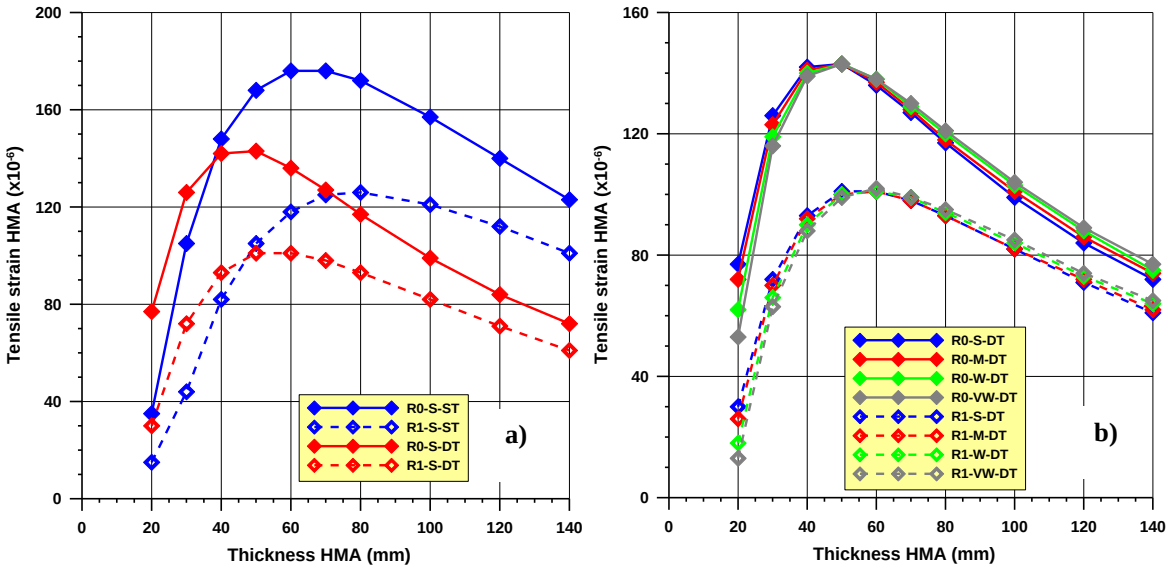


**Fig. 4**. Tensile strain versus **HMA** thickness: a) sections **R0** and **R1** materials, **ST** and **DT** with strong subgrade; b) sections **R0** and **R1** materials, **DT** with **S**, **M**, **W** and **VW** subgrades.

*3.1.3. Effect of material characteristics*

*Effect of subgrade soils*

As was expected, the elastic deflections on the **HMA** wearing course, in the **BSM** base course and in the subgrade upper fibres increase as the stiffness of the subgrade decreases (Table 5). In Fig. 3a, for example, the most rigid subgrade, **S,** produces smaller deflections than the other three, **M**, **W** and **VW**. Fig. 5a and 5b are **3D** representations of the contour of deflections (z displacement) produced in sections **P1**-**R0**, **S** (Strong) and **VW** (Very weak) subgrades, respectively, and with **DT** load. Fig. 6a and 6b are **3D** representations of the displacements produced in section **P1**-**R1**, **S** (Strong) and **VW** (Very weak) subgrades, respectively, and with **DT** load. As can be clearly seen, in both figures, much higher elastic deflections are produced in the section with the least rigid subgrade (**VW**). Moreover, this behaviour is evident on the subgrade vertical strain results (Table 5), and the $SR_{max}$ values are lower with the most rigid subgrade (Table 5).

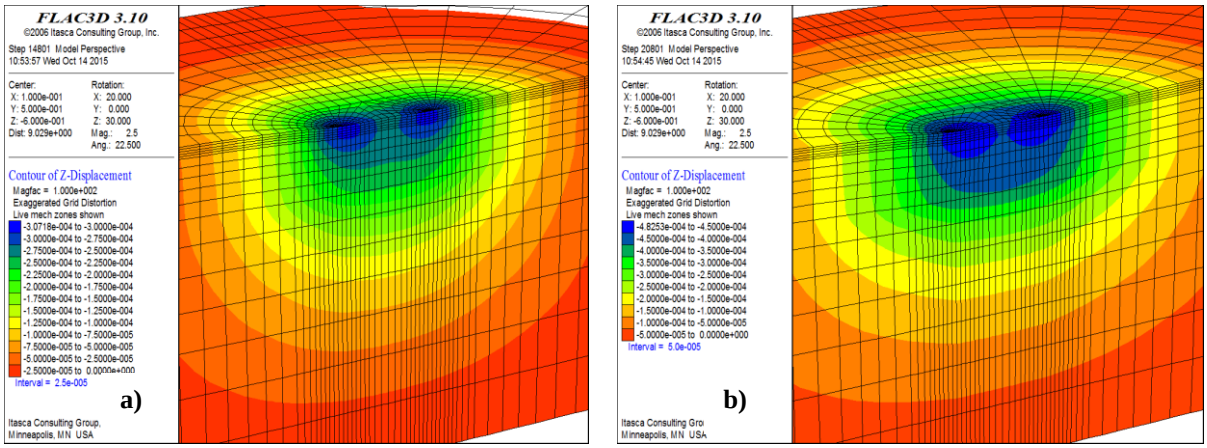


**Fig. 5**. Displacements (m): a) Section **P1-R0-S-DT**; b) Section **P1-R0-VW-DT.**

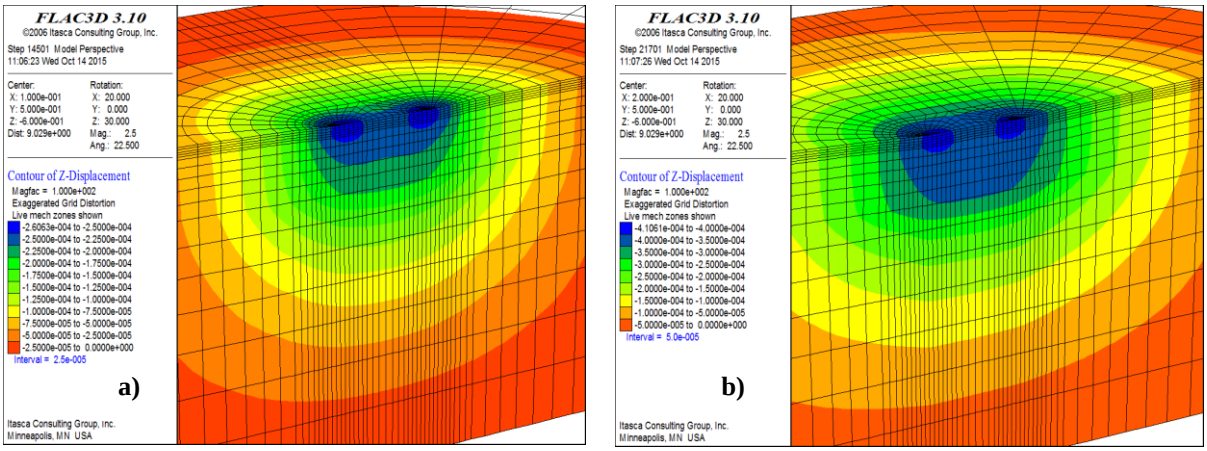


**Fig. 6**. Displacements (m): a) Section **P1-R1-S-DT**; b) Section **P1-R1-VW-DT.**

Again, an exception to this clear-cut behaviour pattern can be found in the tensile strains produced in the **HMA** wearing course. Accordingly, with pavement **P1**, **ST** load and **R1** material, the tensile strain increases as the subgrade stiffness increases (Fig. 3d). This occurs as well with **DT** load and **R0** and **R1** materials. In Fig. 4b, this behaviour can be observed in the four subgrade soils, with **DT** load and **R0** and **R1** materials. Accordingly, below the critical thickness, the tensile strain increases with increasing subgrade stiffness, whereas above the critical thickness, the tensile strain decreases with increasing subgrade stiffness.

*Effect of BSM base course*

If the other three factors remain invariable, (**HMA** thickness, load configuration and subgrade), pavement responses are always lower with material **R1**—e.g., in the **BSM** with 1% cement (Fig. 3a, 3b, 3c, 3d and 3e). In Fig. 4a and 4b, we can observe that the tensile strains

in the **HMA** wearing courses are always fewer with **R1** material. If Fig. 5a and 5b are compared to Fig. 6a and 6b, it is evident that a greater deflection occurs in the sections containing **R0** materials. For example, in section **P1-R0** with subgrade **S**, the maximum surface deflection in the dual tyre zone is roughly equal to 307 μm, whereas in section **P1-R1,** it is only 260 μm. Moreover, the $SR_{max}$ values are lower in **BSM** with 1% cement (**R1**) (Table 5). Therefore, as is logical, the structural capacity of the pavement is greater when the stiffest material **R1** is used.

*3.2. Resilient Modulus*

*3.2.1. Subgrade*

Fig. 7 shows the variation of $M_r$ in sections **P1-RO**, **P1-R1**, **P2-RO** and **P2-R1** with **S** (Strong) and **VW** (Very Weak) subgrades. First, it can be observed that $M_r$ increases with depth. Second, the $M_r$ of the very weak (**VW)** subgrade ranges between 5 MPa (upper fibre) and 30 MPa, whereas those corresponding to the resistant subgrade (**S**) range between 80 MPa (upper fibre) and 110 MPa. In the third place, it is observed that, given equal conditions, the $M_r$ of the subgrade is greater with **HMA** thickness equal to 80 mm (**P2**).

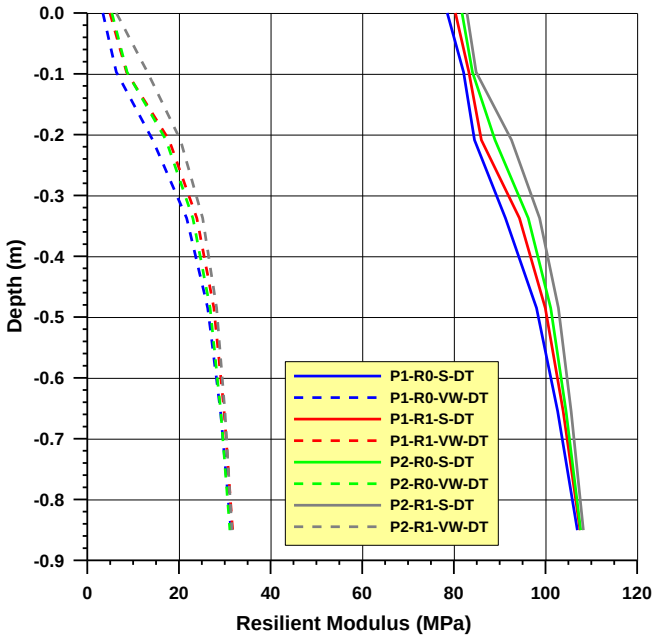


**Fig. 7**. Resilient modulus in the subgrade (Subgrade **S** and **VW**, **DT**).

*3.2.2. BSM base course*

Fig. 8 shows the *Mr* variation in the **BSM** base course for the two types of soils in sections **P1-RO**, **P1-R1**, **P2-RO** and **P2-R1**. Contrary to the previous case, as the depth of the **BSM** base course increases, $M_r$ diminishes. The section **P1-R1-S-DT** is the one that exhibits the highest $M_r$ values, ranging from approximately 700 MPa (lower fibre) to 1300 MPa (upper fibre). The section with the lowest values is **P2-R0-VW-DT**. These values fluctuate between approximately 450 MPa (lower fibre) and 650 MPa (upper fibre). Logically, the $M_r$ values are higher in the section with a **BSM** base course material type **R1** (with 1% cement) and subgrade **S** (Strong). Finally, under equal conditions, the $M_r$ of the **BSM** base course is greater with **HMA** thickness equal to 40 mm (**P1**).

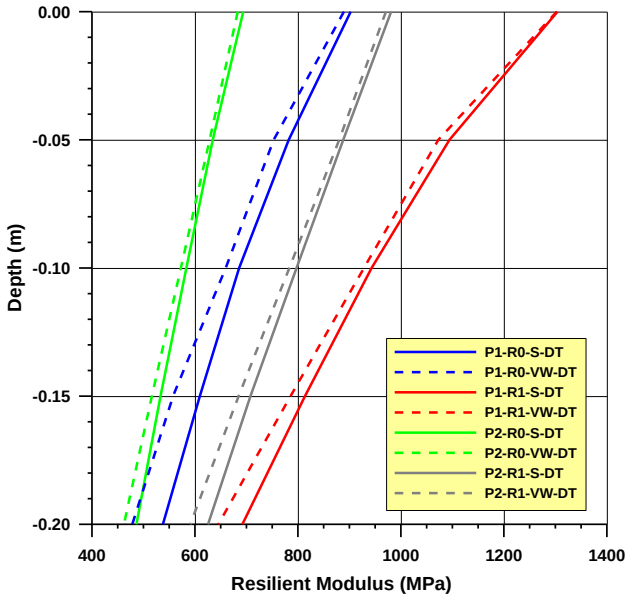


**Fig. 8**. Resilient modulus in the **BSM** base course (Subgrade **S** and **VW**, **DT**).

It is very important to explain that to avoid a negative bulk stress ($\Theta$) and consequently meaningless $M_r$ values, in some cases, $\sigma_3$ was set to 0 while maintaining the same $\sigma_1$. This means that $M_r$ depends only on $\sigma_1$. This stress modification is necessary because no real solution exists for $\theta^{k_2}$ when $\theta$ is negative and $k_2$ is smaller than 1. For example, in **P1-R1-S-DT** section lower fibre, $\Theta=\sigma_1+2\sigma_3=100+2(0)=100$ kPa. Accordingly, applying equation 1, $M_r=150(100)^{0.33}=685$ MPa.

*3.3. BSM Stress Ratios*

To calculate the **BSM** stress ratios, in equation 4, the *c* and $\phi$ values for **R0** and **R1** materials shown in Table 1 were employed. Thus, the next expressions were obtained:

$$SR_{R0} = \frac{\sigma_d}{\sigma_{d,f}} = \frac{\sigma_1 - \sigma_3}{3.28\sigma_3 + 0.63} \quad (6)$$

$$SR_{R1} = \frac{\sigma_d}{\sigma_{d,f}} = \frac{\sigma_1 - \sigma_3}{1.96\sigma_3 + 1.33} \quad (7)$$

where $SR_{R0}$ and $SR_{R1}$ are the stress ratios for **R0** and **R1** materials, respectively. In equations 6 and 7, for the same $\sigma_1$ and $\sigma_3$ values, $SR_{R0}$ will be lower than $SR_{R1}$.

Table 6 lists the high, low and average values of principal stresses $\sigma_1$ induced in the **BSM** base course upper and lower fibres for **P1** and **P2** pavements, resistant subgrade (**S**) and dual tyres (**DT**). Moreover, the minor stresses $\sigma_3$ caused in the same points are presented. In both **R0** and **R1** materials, $\sigma_1$ values are in compression (+ notation). Nevertheless, in sections **P1-R0** and **P1-R1**, $\sigma_3$ values are in compression in the upper fibres (+ notation) and are in traction in the lower fibres (- notation). In addition, in Table 6 the $\sigma_d$, $\sigma_{df}$ and *SR* values are exposed.

**Table 6**. Stresses and stress ratios induced in the **BSM** upper and lower fibres. Sections **P1-R0**; **P1-R1**; **P2-R0** and **P2-R1** with strong subgrade (**S**) and dual tyres (**DT**).

| **BSM** | | **Range value** | **P1** | | | | | **P2** | | | | |
|---|---|---|---|---|---|---|---|---|---|---|---|---|
| | | | $\sigma_1$ (MPa) | $\sigma_3$ (MPa) | $\sigma_d$ (MPa) | $\sigma_{df}$ (MPa) | *SR* | $\sigma_1$ (MPa) | $\sigma_3$ (MPa) | $\sigma_d$ (MPa) | $\sigma_{df}$ (MPa) | *SR* |
| R0 | Upper fibre | High | 0.479 | 0.075 | 0.404 | 0.875 | 0.462 | 0.250 | - 0.010 | 0.260 | 0.596 | 0.435 |
| | | Low | 0.450 | 0.060 | 0.390 | 0.826 | 0.472 | 0.225 | - 0.020 | 0.245 | 0.563 | 0.434 |
| | | Average | 0.465 | 0.068 | 0.397 | 0.851 | 0.467 | 0.238 | - 0.015 | 0.253 | 0.581 | 0.435 |
| | Lower Fibre | High | 0.150 | - 0.100 | 0.250 | 0.301 | 0.828 | 0.100 | - 0.070 | 0.170 | 0.399 | 0.425 |
| | | Low | 0.100 | - 0.108 | 0.208 | 0.275 | 0.752 | 0.075 | - 0.074 | 0.149 | 0.388 | 0.384 |
| | | Average | 0.125 | - 0.104 | 0.229 | 0.289 | 0.792 | 0.088 | - 0.072 | 0.159 | 0.395 | 0.404 |
| R1 | Upper fibre | High | 0.513 | 0.075 | 0.438 | 1.480 | 0.297 | 0.291 | 0.000 | 0.291 | 1.333 | 0.219 |
| | | Low | 0.500 | 0.050 | 0.450 | 1.431 | 0.315 | 0.275 | - 0.020 | 0.295 | 1.293 | 0.229 |
| | | Average | 0.507 | 0.063 | 0.444 | 1.453 | 0.306 | 0.283 | - 0.010 | 0.293 | 1.310 | 0.224 |
| | Lower Fibre | High | 0.150 | - 0.150 | 0.300 | 1.038 | 0.294 | 0.050 | - 0.100 | 0.150 | 1.136 | 0.132 |
| | | Low | 0.100 | - 0.151 | 0.251 | 1.035 | 0.243 | 0.075 | - 0.105 | 0.180 | 1.126 | 0.160 |
| | | Average | 0.125 | - 0.151 | 0.276 | 1.035 | 0.267 | 0.063 | - 0.103 | 0.165 | 1.129 | 0.146 |

In Table 6, it can be observed that, in general, there is not much difference between the $\sigma_d$ values obtained with **R0** and **R1** materials. For example, in the **P1-R1** section, the $\sigma_d$ average values are 0.444 MPa (upper fibre) and 0.276 MPa (lower fibre), whereas in the **P1-R0** section, the $\sigma_d$ average values are 0.397 MPa (upper fibre) and 0.229 MPa (lower fibre). Nevertheless, there is an important difference between the $\sigma_{df}$ values obtained with **R0** and **R1** materials. For instance, in the **P2-R1** section, the $\sigma_{df}$ average values are 1.129 MPa (lower fibre) and 1.310 MPa (upper fibre), whereas in the **P2-R0** section, the $\sigma_d$ average values are 0.395 MPa (lower fibre) and 0.581 MPa (upper fibre). Therefore, $\sigma_d$ values are reasonably similar in **R0** and **R1** materials; but $\sigma_{df}$ values are higher in **R1** materials. For this reason, **R1** materials have lower stress ratios. Moreover, in Table 6, it can be observed that in **P2** pavement with an 80 mm **HMA** wearing course, the $\sigma_d$ and $\sigma_{df}$ stresses are lower than those in **P1** pavement with only a 40 mm **HMA** wearing course. That indicates lower stress ratios in the **P2** pavement.

On the other hand, Fig. 9 and 10 are 3D representations of the **BSM** Stress Ratio variation. In any case, the critical points are located at the midpoint between the wheels. In Fig. 9a (**P1-R0** section), the maximum $SR_{R0}$ value is found in the **BSM** base course lower fibre, slightly to the left of the tyre (0.700–0.777 range). Therefore, in this section, very high **PD** values will occur. In contrast, in Fig. 9b (**P1-R1** section), the maximum $SR_{R1}$ value occurs in the base course upper fibre slightly to the right of the tyre (0.300–0.314 range). In all probability, in this section, lower **PD** values will be induced. In Fig. 10b (**P2-R0** material), the maximum $SR_{R0}$ values are generated in the upper fibre of the layer (0.400–0.441 range). In this section, high **PD** values will probably be created. In Fig. 10b (**P2-R1** section), the maximum $SR_{R1}$ value appears only in the upper part (0.225–0.234 range). Consequently, in this section, **PD** values will be very low.

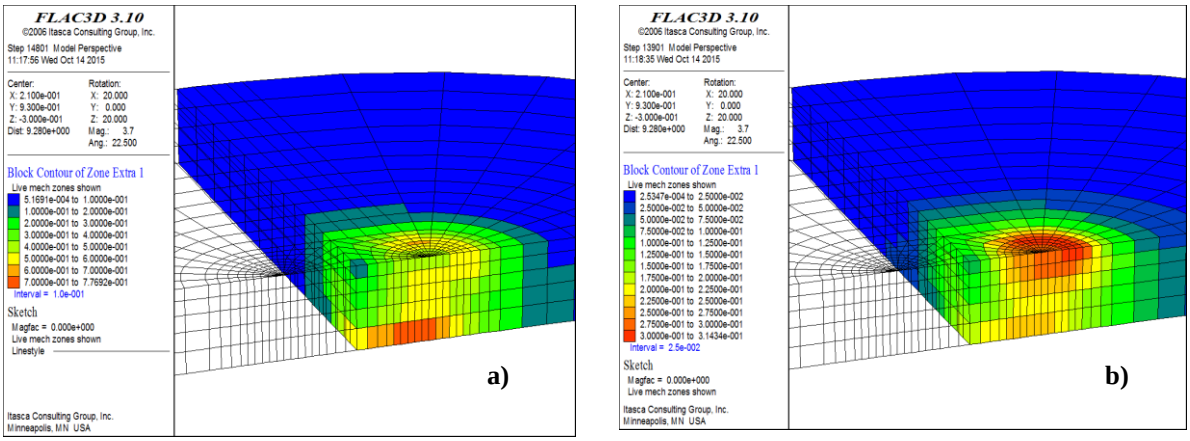


**Fig. 9**. *SR* in the **BSM** base course: a) Section **P1-R0-S-DT**; b) Section **P1-R1-S-DT.**

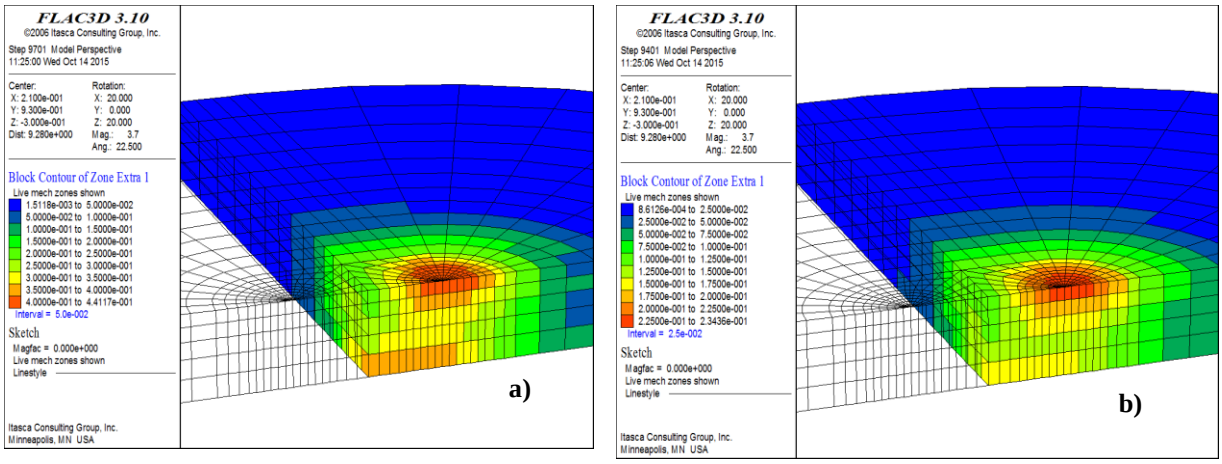


**Fig. 10**. *SR* in the **BSM** base course: a) Section **P2-R0-S-DT**; b) Section **P2-R1-S-DT.**

### *3.4. BSM Rutting Resistance*

Equation 3 was used to estimate the cumulative permanent deformation $\varepsilon_p$ (%) in the **BSM** base course. Fig. 11a shows the $\varepsilon_p$ (%) curves for the four different cases described above versus the number of single axles of 88 kN (**N**).

Clearly, the cumulative permanent deformation increases as the maximum stress ratio increases. The lowest $\varepsilon_p$ (%) value occurs on curve **P2-R1** corresponding to an **HMA** thickness of 80 mm and **BSM** with 1% cement. The highest $\varepsilon_p$ (%) value is found on curve **P1-R0** of **HMA** equal to 40 mm and **BSM** material without cement. The curves show a part in which the relationship between the logarithm of $\varepsilon_p$ (%) and the logarithm of *N* is linear. In all of them, there is a starting point at which $\varepsilon_p$ (%) increases exponentially, which would

indicate that the material is entering a tertiary zone of deformation. On curve **P2-R1**, this point is reached with $1 \times 10^7$ $N$ and 0.15%$\varepsilon_p$. On curve **P1-R1**, it is reached with $1 \times 10^6$ $N$ and 0.4%$\varepsilon_p$. On curve **P2-R0**, it is achieved with $1 \times 10^5$ $N$ and 0.7%$\varepsilon_p$, and on curve **P1-R0**, it is reached with $1 \times 10^4$ $N$ and 2.0%$\varepsilon_p$.

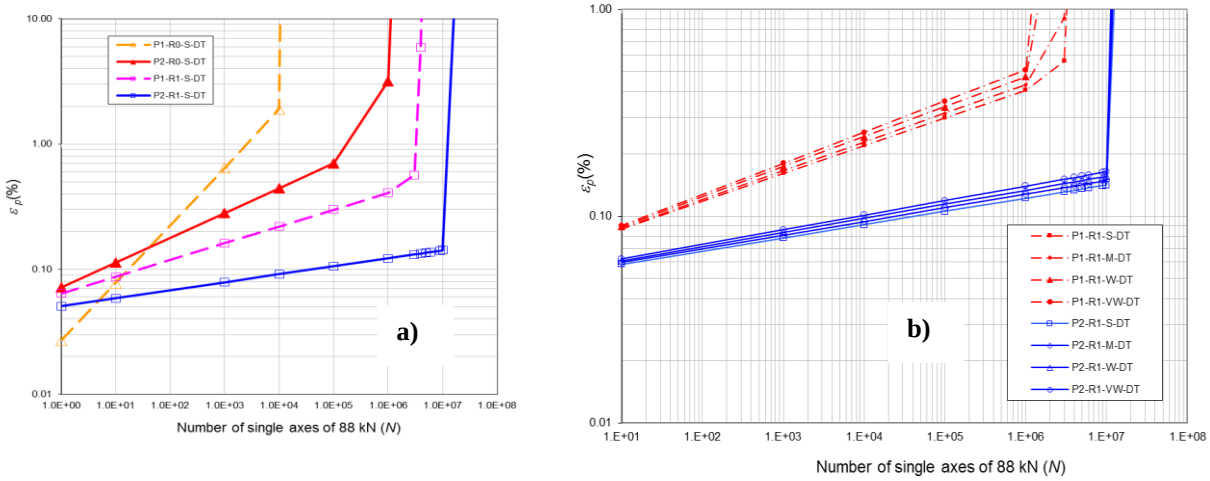


**Fig. 11**. Cumulative permanent deformation in the **BSM** base course: a) Strong Subgrade-Dual Tyres; b) R1 material-Dual Tyres.

Fig. 11b represents the $\varepsilon_p$ (%) curves for material **R1** and dual tyres. In these curves, the two pavement types **P1** and **P2** are shown separately with the four types of subgrade. It can be observed that with pavement **P2** and material **R1**, considering different types of subgrade does not significantly affect the service life of the pavement section. In other words, there is little difference between the $\varepsilon_p$ (%) values generated on the four curves corresponding to the different types of subgrade. Thus, for $1 \times 10^7$ $N$**,** they all show a permanent deformation under 0.20%$\varepsilon_p$. The same behaviour is observed with pavement **P1** and material **R1**, because for $1 \times 10^6$ $N$, the permanent deformation is less than 0.5%$\varepsilon_p$.

In South Africa, according to Liebenberg and Visser [13,14], the permanent deformation failure criterion adopted for rural roads is usually a 20 mm rut depth on the pavement surface. Further, research [18] has shown that approximately 80% of the **PD** observed on the surface originated from within the **BSM** layer whereas the remaining 20%

would be from the other layers of the pavement structure. This relative permanent deformation distribution probably differs in the current pavement of an **HMA** wearing course 40–80 mm thick and a **BSM** base course 200 mm thick over a subgrade. For this reason, the following sensitivity analysis will be conducted considering that 80%, 60%, 40% and 20% of the **PD** on the surface originated from within the **BSM** base course.

On the other hand, the failure criterion is applied to category **C** roads that carry 0.3 to 1 million equivalent standard single-axle loads of 80 kN (0.3 to 1 **MESA**), even though the maximum axle load is 88 kN [6,7]. A load equivalent factor (*LEF*) represents the relative damage caused by axle load *P* compared to a 80 kN single axle load and can be obtained by means of the following expression [7]:

$$LEF = \left(\frac{P}{80}\right)^4 \tag{8}$$

where *P* is any axle load for which equivalence is required (kN), 80 is the equivalent standard load, and 4 is the damage exponent. In this particular case, a 88 kN axle load is equivalent to 1.46 single-axle loads of 80 kN.

Table 7 shows the millions of single-axle loads of 80 kN ($N_{PD}$ expressed in **MESA**) to fail due to rutting for the cases of 80, 60, 40 and 20% **PD** produced within the **BSM** base course.

**Table 7**. Number of **MESA** until failure due to permanent deformation and fatigue.

| Section | **BSM** | | | | | **HMA** |
|---|---|---|---|---|---|---|
| | $N_{PD}$ (MESA) | | | | $N_f$ (MESA) | $N_{fa}$ (MESA) |
| | 80% **PD** (16 mm rut) | 60% **PD** (12 mm rut) | 40% **PD** (8 mm rut) | 20% **PD** (4 mm rut) | | |
| P1-R0 | 0.01 | | | | 2.61 | 2.30 |
| P1-R1 | 7.30 | | | | 60.28 | 10.85 |
| P2-R0 | 1.46 | | | 1.02 | 8.60 | 4.67 |
| P2-R1 | 21.90 | | | | 373.19 | 10.85 |

In Table 7, it is shown that for sections **P1-R0**, **P1-R1** and **P2-R1**, the four percentages of **PD** have the same **MESA**; therefore, the **PD** percentages do not affect the service life. For section **P2-R0**, the $N_{PD}$ are equal only for 80, 60 and 40% **PD**. Only section **P1-R0** has a $\mathbf{N_{PD}}$

below 0.3 **MESA** for category **C** roads. Sections **P1-R1**, **P2-R0** and **P2-R1** are always above 1 **MESA** for category **C** roads.

Hence, section **P2-R1** is the one that resists the highest $N_{PD}$, whereas section **P1-R0** is the one that resists the lowest $N_{PD}$. The sections with material **R1** have a greater resistance to **PD** than the sections containing material **R0**. Increasing the thickness of the wearing course from 40 mm to 80 mm improves resistance to **PD**.

*3.5. BSM Fatigue Resistance*

Equation 5 was used to estimate the fatigue life ($N_f$ expressed in **MESA**) of **BSM** base course for the four previously analysed cases. In Table 7, it can be seen that section **P1-R0** has the poorest behaviour to fatigue and section **P2-R1** has the best behaviour. The sections containing material **R1** behave better than those with material **R0**. Increasing the thickness of the **HMA** wearing course from 40 mm to 80 mm improves the **BSM** base course fatigue resistance. In all cases, **BSM** base courses fail because of **PD** before they succumb to fatigue.

Nevertheless, it is necessary to check whether the failure occurs first owing to the **HMA** fatigue rather than **BSM** base course in any of the sections. This can be accomplished using the fatigue law $N_{fa}$=1.1867 x $10^{-8}$ $\varepsilon^{-3.67}$ employed in Spain to test **HMA** [19]. This law was obtained by means of displacement controlled tests, which are more applicable to **HMA** layers with a relatively low thickness, commonly used in lightly trafficked rural roads. Table 7 shows the **HMA** number of cycles until fatigue failure ($N_{fa}$ expressed in **MESA**). In the four cases, the **HMA** wearing courses will experience fatigue failure before the **BSM** base courses. Finally, with the exception of section **P2-R1** (the section with the thickest **HMA** wearing course and the stiffest **BSM** base course), failure occurs from rutting of the **BSM** base courses before fatigue of the **HMA** wearing courses.

## 4. Conclusions

Based on the results of this research, the following conclusions can be drawn:

- The responses of the pavement are more satisfactory in cases with an 80 mm thick **HMA** wearing course, with the exception of **HMA** tensile strain in sections **P2-R0** and **P2-R1** with a single tyre and **P2-R1** with dual tyres. Better structural behaviour was also obtained with dual tyres, except for the **HMA** wearing course tensile strain in section **P1-R1**.
- The responses of the pavement also decrease as the subgrade stiffness increases, except in the case of **HMA** wearing course tensile strain in sections **P1-R0** and **P1-R1** with dual tyres and in **P1-R1** with a single tyre.
- In an **HMA** wearing course situated over a **BSM** base course, there is a "critical thickness" with a maximum tensile strain.
- The responses are more satisfactory with **BSM** base courses with material **R1** containing 1% cement.
- The $M_r$ of the subgrade increases with depth, whereas that of the **BSM** base course materials decreases. The $M_r$ of the subgrade is higher with an 80 mm **HMA** wearing course, whereas the corresponding value of the **BSM** base course is greater with 40 mm **HMA**. The $M_r$ of the **BSM** base course is higher in layers containing **R1** materials and with a resistant subgrade (**S**).
- In a 88 kN single axle with dual tyres, the maximum *SR* values are found at the following critical points of the **BSM** base course:
    - Section **P1-R0** in the lower fibre to the left of the tyre centre.
    - Section **P1-R1** in the upper fibre to the right of the tyre centre.
    - Section **P2-R0** in the upper fibre underneath the tyre.
    - Section **P2-R1** in the upper fibre underneath the tyre.
- The smallest *SR* and the lowest permanent deformation occur jointly with an 80 mm thick **HMA** wearing course, **BSM** base course material **R1** and resistant subgrade (**S**).

- In the section with **BSM** base course material **R1**, the subgrade stiffness does not significantly affect the resistance to the permanent deformation of the **BSM** material.
- With resistant subgrade (**S**), the **BSM** base course of section **P1-R0** is the one with the poorest fatigue behaviour, and section **P2-R1** exhibits the best behaviour.
- The **BSM** base course materials begin to fail from rutting before they fail from fatigue. The failure of pavement sections may be first attributed to rutting in the **BSM** and subsequently to **HMA** fatigue, except in section **P2-R1**. Therefore, it can be stated that in these types of **BSM** recycled in situ with asphalt emulsion, as a design parameter, resistance to **PD** is more critical than fatigue resistance.
- Pavement section **P1-R1** containing **BSM** is apt for use in South African Category **C** roads.
- It is crucial to validate the numerical simulation obtained in this research by comparing the measurement results of in-field pavement responses to the results of the corresponding numerical simulation.

## Acknowledgments

The authors are grateful to the Ministry of Science and Innovation of the Spanish government for providing the financial support for this research paper within the framework of the FÉNIX Research Project (Strategic investigation for safer and more sustainable roads), subsidized by the program CENIT 2007 of the Centro para el Desarrollo Tecnológico e Industrial (CDTI).

## References

[1]. Thomas TW, May RW. Mechanistic-Empirical Design Guide Modelling of Asphalt Emulsion Full Depth Reclamation Mixes. In: Proceedings of Transportation Research

Board 86th Annual Meeting (CD-ROM), Transportation Research Board, Washington, D.C; 2007.

[2]. Jenkins KJ, Long FM, Ebels LJ. Foamed bitumen mixes=shear performance. Int. J. Pavement Eng. 2007; 8(2): 85-98.

[3]. Ebels LJ. Characterisation of Material Properties and Behaviour of Cold Bituminous Mixtures for Road Pavements. PhD thesis. Stellenbosch University, South Africa; 2008.

[4]. Jenkins KJ, Yu M. Cold-Recycling Techniques Using Bitumen Stabilization: Where is This Technology Going? In: Geotechnical Special Publication 191, Road Pavement Material Characterization and Rehabilitation, ASCE; 2009. p. 191-200

[5]. Collings D, Jenkins K. The Long-Term Behaviour of Bitumen Stabilised Materials (BSMs). In: 10th Conference on Asphalt Pavements for Sothern Africa, KwaZulu-Natal, South Africa; 2011.

[6]. Asphalt Academy. Technical Guideline: Bitumen Stabilised Materials. A Guideline for the Design and Construction of Bitumen Emulsion and Foamed Bitumen Stabilised Materials. TG 2 Second edition, South Africa; 2009.

[7]. South African National Roads Agency. South African Pavement Engineering Manual. South Africa, 2013.

[8]. Itasca Consulting Group, Inc. FLAC3D (Fast Lagrangian Analysis of Continua in 3 Dimensions). Version 3.10. User's manual. Minneapolis, MN; 2006.

[9]. Haidi MNS, Bodhinayake B.C. Non-linear finite element analysis of flexible pavements. Adv. Eng. Software 2003; 34(11-12): 657-662.

[10]. Thompson MR, Robnett QL. Resilient Properties of Subgrade Soils. J. Transp. Eng. 1979; 105(1): 71-89.

[11]. Elliot RP, Thompson MR. Illi-Pave Mechanistic Analysis of AASHO Road Test Flexible Pavements. Transp. Res. Rec. 1985; 1043: 39-49.

[12]. Thompson MR, Elliot RP. Illi-Pave-Based Response Algorithms for Design of Conventional Flexible Pavements. Transp. Res. Rec. 1985; 1043: 50-57.

[13]. Liebenberg JJE, Visser AT. Stabilization and Structural Design of marginal Materials for Use in Low-Volume Roads. Transp. Res. Rec. 2003; 1819: 166-172.

[14]. Liebenberg JJE, Visser AT. Towards a mechanistic structural design procedure for emulsion-treated base layers. J. South Afr. Inst. Civil Eng. 2004; 46(3): 2-8.

[15]. Twagira ME, Jenkins KJ, Ebels LJ, Characterization of Fatigue Performance of Selected Cold Bituminous Mixes. In: 10th International Conference on Asphalt Pavements, Québec, Canada; 2006.

[16]. Huang YH. Critical Tensile Strain in Asphalt Pavements. Transportation Engineering Journal 1973; 99(3): 553-568.

[17]. Freeme CR, Marais CP. Thin Bituminous Surfaces: Their Fatigue Behavior and Prediction. Highway Research Board 1973. Special Report 140: 158-182.

[18]. Liebenberg JJE. A Structural Design Procedure for Emulsion Treated Pavement Layers. Master of Engineering dissertation, University of Pretoria, 2003

[19]. Ministerio de Fomento. Secciones de firme de la instrucción de carreteras. Ediciones Liteam, Madrid, Spain; 2003.